

ACCEPTED MANUSCRIPT

Robust Simultaneous Myoelectric Control of Multiple Degrees of Freedom in Wrist-Hand Prostheses by Real-Time Neuromusculoskeletal Modeling

To cite this article before publication: Massimo Sartori *et al* 2018 *J. Neural Eng.* in press <https://doi.org/10.1088/1741-2552/aae26b>

Manuscript version: Accepted Manuscript

Accepted Manuscript is “the version of the article accepted for publication including all changes made as a result of the peer review process, and which may also include the addition to the article by IOP Publishing of a header, an article ID, a cover sheet and/or an ‘Accepted Manuscript’ watermark, but excluding any other editing, typesetting or other changes made by IOP Publishing and/or its licensors”

This Accepted Manuscript is © 2018 IOP Publishing Ltd.

During the embargo period (the 12 month period from the publication of the Version of Record of this article), the Accepted Manuscript is fully protected by copyright and cannot be reused or reposted elsewhere.

As the Version of Record of this article is going to be / has been published on a subscription basis, this Accepted Manuscript is available for reuse under a CC BY-NC-ND 3.0 licence after the 12 month embargo period.

After the embargo period, everyone is permitted to use copy and redistribute this article for non-commercial purposes only, provided that they adhere to all the terms of the licence <https://creativecommons.org/licenses/by-nc-nd/3.0>

Although reasonable endeavours have been taken to obtain all necessary permissions from third parties to include their copyrighted content within this article, their full citation and copyright line may not be present in this Accepted Manuscript version. Before using any content from this article, please refer to the Version of Record on IOPscience once published for full citation and copyright details, as permissions will likely be required. All third party content is fully copyright protected, unless specifically stated otherwise in the figure caption in the Version of Record.

View the [article online](#) for updates and enhancements.

1 2 Robust Simultaneous Myoelectric Control of Multiple Degrees of Freedom in 3 Wrist-Hand Prostheses by Real-Time Neuromusculoskeletal Modeling 4 5

6 Massimo Sartori^{1,*}, Guillaume Durandau¹, Strahinja Došen², and Dario Farina³
7
8

9 ¹Department of Biomechanical Engineering, University of Twente, NETHERLANDS
10

11 ² Department of Health Science and Technology, Faculty of Medicine, Aalborg University, DENMARK
12

13 ³Department of Bioengineering, Imperial College London, UNITED KINGDOM
14

15 *Address of correspondence
16

17 Massimo Sartori, Ph.D.
18

19 Assistant Professor
20

21 University of Twente
22

23 TechMed Centre
24

25 Faculty of Engineering Technology
26

27 Department of Biomechanical Engineering
28

29 Building Horsting - Room W106 - P.O. Box 217
30

31 7500 AE Enschede, The Netherlands
32

33 Email: m.sartori@utwente.nl
34

35 **Keywords:** electromyography; EMG-driven modeling; muscle force; musculoskeletal modeling; myoelectric
36 prosthesis; joint moment; real-time; transradial amputee.
37

38 ABSTRACT 39

40 **Objectives:** Robotic prosthetic limbs promise to replace mechanical function of lost biological extremities
41 and restore amputees' capacity of moving and interacting with the environment. Despite recent advances in
42 biocompatible electrodes, surgical procedures, and mechatronics, the impact of current solutions is hampered
43 by the lack of intuitive and robust man-machine interfaces. **Approach:** Based on authors' developments, this
44 work presents a biomimetic interface that synthetizes the musculoskeletal function of an individual's
45 phantom limb as controlled by neural surrogates, i.e. electromyography-derived neural activations. With
46 respect to current approaches based on machine learning, our method employs explicit representations of the
47 musculoskeletal system to reduce the space of feasible solutions in the translation of electromyograms into
48 prosthesis control commands. Electromyograms are mapped onto mechanical forces that belong to a
49 subspace contained within the broader operational space of an individual's musculoskeletal system. **Results:**
50 Our results show that this constraint makes the approach applicable to real-world scenarios and robust to
51 movement artefacts. This stems from the fact that any control command must always exist within the
52 musculoskeletal model operational space and be therefore physiologically plausible. The approach was
53 effective both on intact-limbed individuals and a transradial amputee displaying robust online control of
54 multi-functional prostheses across a large repertoire of challenging tasks. **Significance:** The development
55 and translation of man-machine interfaces that account for an individual's neuromusculoskeletal system
56 creates unprecedented opportunities to understand how disrupted neuro-mechanical processes can be
57 restored or replaced via biomimetic wearable assistive technologies.
58

1
2 53 INTRODUCTION
3

4 54 The accurate and robust decoding of human limb motor function from recordings of the underlying
5 55 neuromuscular activity (i.e. brain, nerve or muscle electrophysiological signals) is a complex, long-standing
6 problem [1–3]. This challenge is central for the development of control paradigms to restore lost motor
7 function in impaired individuals. Despite the advances in electromyography (EMG) and in surgical
8 procedures such as targeted muscle reinnervation [4], myoelectric prostheses still have limited clinical and
9 commercial impact [5], i.e. upper limb prostheses have peak abandonment rates between 40%-50% and
10 average rates around 25% among users [2].
11
12

13 61 Current myoelectric prosthesis control methods rely on machine learning where pattern recognition and
14 62 linear/non-linear regressions map EMGs into limb kinematics [6,7]. However, the human neuro-musculo-
15 63 skeletal system is characterized by multiple muscles spanning a single joint. Therefore, the same joint
16 64 rotation can be generated by different EMG patterns that can further vary across individuals, training
17 65 conditions, arm postures, or tasks [8]. The mapping functions learned in a specific condition (i.e. low force
18 66 tasks, or specific arm posture) do not necessarily generalize to novel conditions (i.e. high force tasks, or
19 67 different arm posture). Furthermore, the mapping from EMG to kinematics is not direct, as assumed in
20 68 machine learning schemes, i.e. limb kinematics is the musculoskeletal system final output generated by
21 69 series of dynamic transformations (transfer functions) in response to control commands (EMG). For this
22 70 reason, a single mapping function between EMGs and joint angular position (current state of the art
23 71 approaches) may not always capture the complexity of all intermediate nonlinear transformations [2,9].
24
25

26 72 A major barrier to natural artificial limb myoelectric control is the limited understanding of the
27 73 biomechanical and neuromuscular mechanisms governing biological joints. Here we propose an interface
28 74 that exploits an individual's broader neuro-mechanical information for device control rather than only the
29 75 underlying electrophysiological signals [1,10]. We record residual forearm EMGs from a transradial amputee
30 76 and intact-limbed individuals, extract EMG-based features of neural activation and concurrently drive
31 77 forward a subject-specific musculoskeletal model of the forearm [11–14]. This enables predicting the
32 78 resulting mechanical moments actuating wrist-hand joints and prescribing them in real-time to a robotic
33 79 multi-functional prosthesis low-level controller.
34
35

36 80 Although recent research demonstrated the possibility of operating EMG-driven musculoskeletal models
37 81 in real-time during dynamic movements [15–17], online EMG-driven modelling has never been developed
38

1
2 82 and applied for the control of multiple degrees of freedom (DOF) robotic limbs. To the best of our
3 knowledge the work presented in this manuscript is the first demonstration of real-time model-based
4
5
6 84 myoelectric prosthesis control on amputee individuals.
7

8 85 Current state of the art work proposed and tested modeling formulations in intact-limbed individuals in
9 isometric conditions and about a single joint DOF, i.e. elbow flexion-extension [18]. Although a real-time
10
11 86 two-DOF upper limb model was recently proposed [19], this was not driven by EMGs but operated via
12 simulated signals. A simplified lumped-parameter model of the hand [20,21] was recently used to compute
13
14 88 wrist and metacarpophalangeal joint flexion/extension angles in a transradial amputee. However, this did not
15 show the ability of controlling a physical prosthesis in real-time. That is, tests involved non-functional static
16 poses where the amputee controls a virtual cursor to reach given targets [20–22]. This is a major limitation.
17
18 90 Without direct proof of physical prosthesis control it is not possible to assess whether a myocontrol method
19 can be realistically employed by the user. Tests based on virtual cursor control would not account for
20
21 92 prosthesis weight, socket pressure, and prosthesis interaction with real objects, which would affect EMG
22 quality, stability, and pose a challenge for control. Tests only involving static poses would not account for
23
24 94 EMG non-stationarities (due to muscle fiber movement relative to electrode pick up areas), which may
25 further affect control performance. Moreover, these tests would not enable understanding whether reported
26
27 96 target reaching times enable prompt control of a physical prosthesis during functional tasks.
28
29

30 99 Importantly, current model-based methods integrate the dynamic equations of motions in order to predict
31 joint angles from EMGs [19,20,23]. As previously demonstrated [23], the numerical integration problem can
32 become stiff, thus displaying numerical instability in the forward dynamic simulation. As a result, due to
33
34 100 numerical integration computational load, state of the art formulations underlie simplified lumped
35 musculoskeletal models with reduced sets of DOFs, limiting translation to more proximal amputations, i.e.
36
37 102 transhumeral. These are major elements hampering robustness in the EMG-driven models currently existing,
38
39 104 which may underpin the current inability of employing EMG-driven musculoskeletal modeling for the real-
40
41 105 time control of robotic limbs.
42
43

44 107 The authors recently demonstrated the ability to establish real-time EMG-driven musculoskeletal models
45 for the online estimation of joint moments about three DOFs simultaneously in the human lower limb [24].
46
47 108 Based on this work, we here translate and embed a large-scale and physiologically-accurate EMG-driven
48
49 109 musculoskeletal model [25] into a new myoelectric control paradigm for a multifunctional robotic wrist-hand
50
51

prosthesis. Unlike state-of-the-art approaches, our method does not integrate the equations of motion (Fig. 1A). We propose a new paradigm where the physical prosthesis is used, instead of a numerical integrator [20], to convert EMG-decoded joint moments into joint angles (Fig. 1B-C). Whether or not it is possible to decode phantom limb joint moments, instead of joint angles, from residual muscle EMGs and concurrently control a physical prosthesis represents an unanswered question. If possible, this would enable fast simulation of large-scale musculoskeletal models and open up to applications requiring the control of many DOFs, especially important for individuals who underwent targeted muscle reinnervation procedures.

We here show that our proposed paradigm is robust to arm postures while enabling seamless wrist-hand prosthesis control across a large repertoire of functionally relevant motor tasks in an individual with transradial amputation. We provide tangible results showing the successful use of a new model-based paradigm in real myoelectric prosthesis control scenarios and real-world situations involving patients. The novel method we propose consistently outperformed the classic two-channel control (representing the commercial benchmark) in all the tests including multiple-DOF tasks as well as single-DOF tasks where the commercial benchmark is expected to be best performing. To the best of our knowledge these results have never been achieved by any study so far.

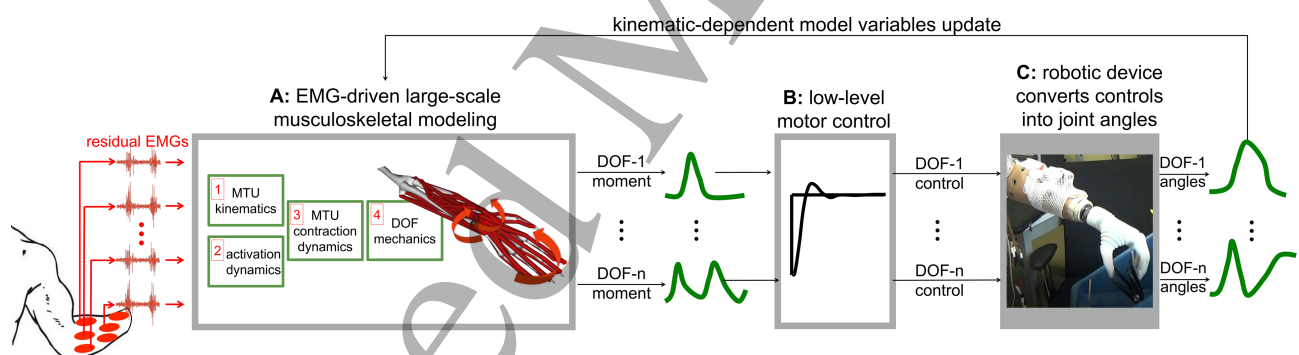


Figure 1. Model-based control schematics for upper limb myoelectric robotic limbs. (A) A large-scale, physiologically correct musculoskeletal model predicts muscle forces of residual forearm muscles as well the resulting joint moments acting on the amputee's phantom limb. (B) Joint moment estimates are converted into prosthesis low-level motor commands. (C) The prosthesis is the physical device that converts EMG-predicted joint forces into joint kinematics, rather than using numerical integration as previously proposed. This enables real-time simultaneous and proportional control multi of multiple degrees of freedom (DOFs) in myoelectric robotic limbs.

1
2 135 **METHODS**
3

4 136 We developed a subject-specific modeling formulation (Figs 1-2) that enabled estimation of wrist-hand
5
6 137 musculoskeletal function in both intact-limbed individuals and transradial amputees as controlled by EMG-
7
8 138 derived neural activations. We demonstrated the ability of using resulting model-based joint moment
9 estimates for the concurrent, real-time control of a myoelectric prosthesis throughout a large repertoire of
10 139 wrist-hand tasks. Our proposed framework schematic is depicted in Figs 1-2 and comprises three major
11 140 components including: EMG-driven musculoskeletal model (Fig. 1A), prosthesis low-level controller (Fig.
12 141 1B-C), and model calibration (Fig. 2). The EMG-driven musculoskeletal model component is developed
13 142 based on previous work from the authors [13–15,26–30] as well as from other groups [31–37].
14
15 143

16 144 Experimental procedures were performed for each individual subject on two consecutive days. During
17 145 the first day, a musculoskeletal model was scaled and calibrated to match each individual's anthropometry
18 146 and force-generating capacity. During the second day, the subject-specific model was employed for the
19 147 online prosthesis control tests across arm configurations. Online control tests were performed with no model
20 148 re-calibration and involved direct comparison with the classic two-channel control benchmark. The
21 149 commercial benchmark was chosen because it provides highest robustness in the control of single-DOFs
22 150 across arm configurations and therefore represents the best means for comparison with respect to our
23 151 proposed method.

24
25 152 First, we describe how motion data were collected and processed for establishing subject-specific
26 153 musculoskeletal models, i.e. see Data Recording and Processing Section. Second, we describe our proposed
27 154 model-based framework components (see EMG-driven Musculoskeletal Model, Prosthesis Low-Level
28 155 Controller and Model Calibration Sections) along with the communication framework that enabled data flow
29 156 between EMG amplifier, prosthetic limb and model-based framework (see System Communication
30 157 Framework Section). Third we describe the online prosthesis control testing procedures (see Experimental
31 158 Tests Section).

32 159

33 160 **Data Recording and Processing**

34 161 Motion capture data were recorded (256Hz) using a seven-camera system (Qualisys, Göteborg, Sweden,
35 162 256Hz) and a set of 18 retro-reflective markers placed on the individual's intact left upper extremity, residual
36 163 right upper extremity, trunk, and pelvis. Data were recorded during one static anatomical pose and used in

conjunction with the open-source software OpenSim [38] to scale a generic upper extremity model of the musculoskeletal geometry [25,39] to match the subject's anthropometry. The musculoskeletal geometry model had six upper extremity DOFs including: shoulder elevation, shoulder adduction-abduction, elbow flexion-extension, forearm pronation-supination, wrist flexion-extension, and first-to-fourth proximal metacarpophalangeal joint flexion-extension. Although the model encompasses all DOFs and muscle-tendon units (MTUs) in the human hand [25], only a subset of these were employed. Specifically, this incorporated a total of 12 MTUs spanning the elbow, wrist and hand joints (Table I). During the scaling process, virtual markers were placed on the generic musculoskeletal geometry model based on the position of the experimental markers from the static pose. The model anthropomorphic properties as well as MTU insertion, origin and MTU-to-bone wrapping points were linearly scaled on the basis of the relative distances between experimental and corresponding virtual markers[38].

EMGs were measured (10KHz) and A/D converted with 12-bit precision using a 256-channel EMG amplifier (OTBioelettronica, Torino, IT). Only eight channels were used for the experiment, i.e. via eight pairs of disposable bipolar electrodes (Ambu, Neuroline 720, DK). Electrodes were placed in the correspondence of eight upper limb muscle groups including: biceps brachii, pronator teres, extensor carpi radialis, extensor carpi ulnaris, extensor digitorum, flexor carpi radialis, flexor carpi ulnaris, flexor digitorum. Placement was performed following SENIAM recommendations with a 10mm inter-electrode distance (measured from each electrode center) [40]. Each individual was initially asked to perform maximal voluntary contractions articulating wrist flexion-extension, forearm pronation-supination, and hand opening-closing. EMGs were high-pass filtered (30Hz), full-wave rectified, and low-pass filtered (6 Hz) using a second-order Butterworth filter. Resulting peak-processed values were used for the subsequent EMG normalization during the real-time myocontrol experimental tests. All tests were performed using a powered multi-functional wrist hand prosthesis (Michelangelo Hand, Ottobock HealthCare GmbH, Duderstadt, DE) equipped with wrist pronation-supination (WPS), flexion-extension (WFE) and hand opening-closing (HOC) motors. The prosthesis can produce two grasp types; the palmar grasp was used (HOC) in the present study. The hand is sensorized with embedded position and force sensors, measuring aperture size, wrist rotation angle and grasping force. The commands to the hand and sensor data from the hand were transmitted through a Bluetooth or TCP/IP connection (100 Hz).

Table I. EMG to MTU mapping. Mapping between experimental electromyograms (EMGs) and

1
2 193 simulated musculotendon units (MTUs)*.

EMGs	Biceps Brachii	Pronator Teres	Extensor Carpi Radialis	Extensor Carpi Ulnaris	Extensor Digitorum	Flexor Carpi Radialis	Flexor Carpi Ulnaris	Flexor Digitorum
MTUs	BIClong, BICshort	PT, PQ	ECRL, ECRB	ECU	EDC	FCR	FCU	FDS, FDPM

9 194 * Musculotendon unit names: biceps brachii long head (BIClong) and short head (BICshort), extensor carpi
10 195 radialis longus (ECRL), extensor carpi radialis brevis (ECRB), extensor carpi ulnaris (ECU), extensor
11 196 digitorum communis (EDC), flexor carpi radialis (FCR), flexor carpi ulnaris (FCU), flexor digitorum
12 197 superficialis (FDS), flexor digitorum profundus (FDPM), pronator quadratus (PQ), and pronator teres (PT).
13 198

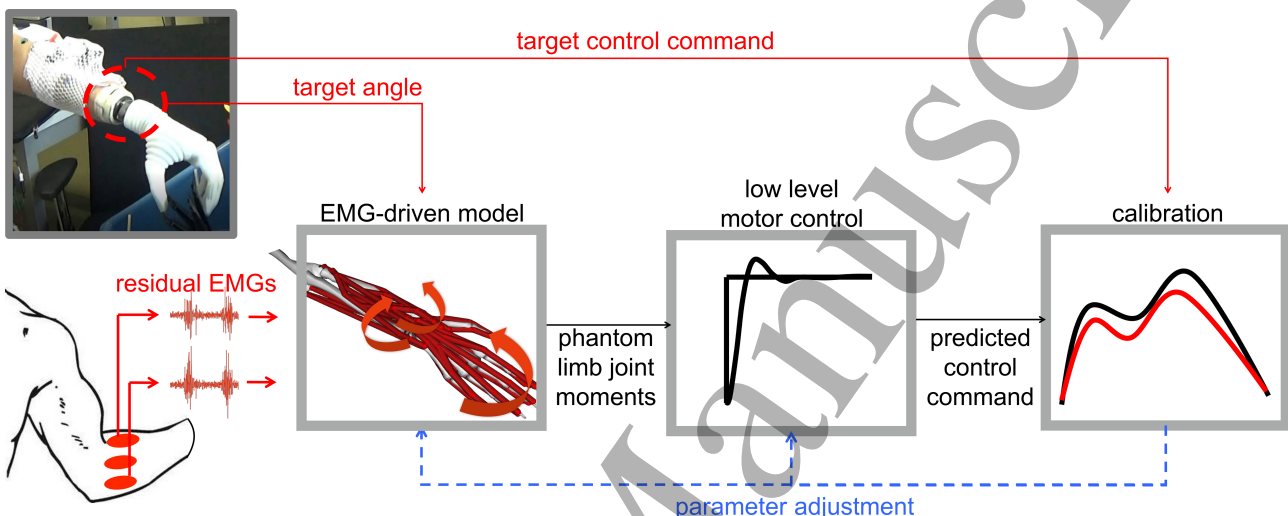
15 199 **EMG-driven Musculoskeletal Model**

16
17 200 Our proposed EMG-driven modeling framework (Fig. 1) receives as an input: (1) EMGs from the amputee's
18 residual limb and (2) prosthesis joint angles. This information is used to compute the mechanical moments
19 201 produced to actuate the amputee's phantom limb and the intact-limbed individuals' wrist-hand. The EMG-
20 202 driven musculoskeletal modeling formulation comprises four main components [13,26,27,41]. The **neural**
21 203 activation component (Fig. 1A.1) converts EMGs into MTU-specific activation using a second order
22 204 muscle twitch model and a non-linear transfer function [13,30,41]. Eight EMG channels were mapped into
23 205 12 MTUs as detailed in Table I. The **MTU kinematics component** (Fig. 2A.2) synthesizes the MTU paths
24 206 defined in the subject-specific geometry model into a set of MTU-specific multidimensional cubic B-splines.
25
26 207 Each B-spline computes MTU kinematics (i.e. MTU length and moment arms) as a function of input
27
28 208 prosthesis joint angles [27]. The **MTU dynamics component** (Fig. 2A.3) solves for the dynamic equilibrium
29
30 209 between muscle fibers and series tendons in the production of MTU force. It employs a Hill-type muscle
31
32 210 model with activation-force-length-velocity relationships informed by MTU length and neural activations
33
34 211 from the previous two components [13,42]. The **joint mechanics component** (Fig. 1A.4) transfers MTU
35
36 212 forces to the skeletal joint level using MTU moment arms. This enables computing joint moments [13].
37
38 213 Unlike state of the art methods, this procedure does not require forward integration of the equations of
39 motion and is done in real-time using a physiologically correct large-scale musculoskeletal model, i.e. no
40
41 214 need for simplification in the underlying musculoskeletal structure being modeled [11].
42
43 215

53 217 54 55 218 **Prosthesis Low-Level Controller**

56
57 219 The joint moments predicted by the EMG-driven model are subsequently converted into prosthesis low-level
58 control commands (Fig. 1B). These are first amplitude-normalized, threshold-processed, and prescribed to
59 220

1
2 221 the prosthesis DOFs individually (Fig. 1C). The prosthesis embedded low-level controller receives input
3 commands and rotates the prosthesis joints with a velocity profile that is proportional to the decoded joint
4 moment. The prosthesis DOF angular kinematics is directly modulated as a function of the input command
5 amplitude. The prosthesis movement emerging from these commands is fed into the EMG-driven model
6 MTU kinematic component (Fig. 1A.2) and used to update the kinematic-dependent state in the
7 musculoskeletal model. This includes skeletal DOF angular position as well as DOF-angle-dependent MTU
8 length, MTU-to-bone wrapping points, and MTU moment arms.
9
10 225
11 226
12 227
13
14
15
16
17
18
19
20
21
22
23
24
25
26
27
28
29
30
31
32 228
33
34 229 **Figure 2. Model calibration procedure.** The real-time EMG-driven model-based controller is calibrated
35 using prosthesis joint motor control commands. During calibration the amputee is instructed to mimic pre-
36 defined motions executed by the prostheses using their own phantom limb. EMG-driven model internal
37 parameters are repeatedly refined, as part of a least-squares optimization procedure, so that the mismatch
38 between EMG-driven model's predicted prosthesis DOF commands and those produced by the prosthesis
39 pre-defined command inputs is minimized.
40
41
42
43
44
45
46
47
48
49
50
51
52
53
54
55
56
57
58
59
60
61
62
63
64
65
66
67
68
69
70
71
72
73
74
75
76
77
78
79
80
81
82
83
84
85
86
87
88
89
90
91
92
93
94
95
96
97
98
99
100
101
102
103
104
105
106
107
108
109
110
111
112
113
114
115
116
117
118
119
120
121
122
123
124
125
126
127
128
129
130
131
132
133
134
135
136
137
138
139
140
141
142
143
144
145
146
147
148
149
150
151
152
153
154
155
156
157
158
159
160
161
162
163
164
165
166
167
168
169
170
171
172
173
174
175
176
177
178
179
180
181
182
183
184
185
186
187
188
189
190
191
192
193
194
195
196
197
198
199
200
201
202
203
204
205
206
207
208
209
210
211
212
213
214
215
216
217
218
219
220
221
222
223
224
225
226
227
228
229
230
231
232
233
234
235
236
237
238
239
240
241
242



34 229 **Figure 2. Model calibration procedure.** The real-time EMG-driven model-based controller is calibrated
35 using prosthesis joint motor control commands. During calibration the amputee is instructed to mimic pre-
36 defined motions executed by the prostheses using their own phantom limb. EMG-driven model internal
37 parameters are repeatedly refined, as part of a least-squares optimization procedure, so that the mismatch
38 between EMG-driven model's predicted prosthesis DOF commands and those produced by the prosthesis
39 pre-defined command inputs is minimized.
40
41
42
43
44
45
46
47
48
49
50
51
52
53
54
55
56
57
58
59
60
61
62
63
64
65
66
67
68
69
70
71
72
73
74
75
76
77
78
79
80
81
82
83
84
85
86
87
88
89
90
91
92
93
94
95
96
97
98
99
100
101
102
103
104
105
106
107
108
109
110
111
112
113
114
115
116
117
118
119
120
121
122
123
124
125
126
127
128
129
130
131
132
133
134
135
136
137
138
139
140
141
142
143
144
145
146
147
148
149
150
151
152
153
154
155
156
157
158
159
160
161
162
163
164
165
166
167
168
169
170
171
172
173
174
175
176
177
178
179
180
181
182
183
184
185
186
187
188
189
190
191
192
193
194
195
196
197
198
199
200
201
202
203
204
205
206
207
208
209
210
211
212
213
214
215
216
217
218
219
220
221
222
223
224
225
226
227
228
229
230
231
232
233
234
235
236
237
238
239
240
241
242

48 236 Model Calibration

50 237 During calibration, the amputee is instructed to activate the muscles in the residual limb mimicking pre-
51
52
53
54
55
56
57
58
59
60
61
62
63
64
65
66
67
68
69
70
71
72
73
74
75
76
77
78
79
80
81
82
83
84
85
86
87
88
89
90
91
92
93
94
95
96
97
98
99
100
101
102
103
104
105
106
107
108
109
110
111
112
113
114
115
116
117
118
119
120
121
122
123
124
125
126
127
128
129
130
131
132
133
134
135
136
137
138
139
140
141
142
143
144
145
146
147
148
149
150
151
152
153
154
155
156
157
158
159
160
161
162
163
164
165
166
167
168
169
170
171
172
173
174
175
176
177
178
179
180
181
182
183
184
185
186
187
188
189
190
191
192
193
194
195
196
197
198
199
200
201
202
203
204
205
206
207
208
209
210
211
212
213
214
215
216
217
218
219
220
221
222
223
224
225
226
227
228
229
230
231
232
233
234
235
236
237
238
239
240
241
242

(normalized velocities) producing the target DOF angles. The **calibration component** (Fig. 2) identifies a number of amputee-specific musculoskeletal parameters that vary non-linearly across individuals because of anatomical and physiological differences. These include: muscle twitch activation/deactivation time constants, EMG-to-activation non-linearity factor, muscle optimal fiber length, tendon slack length, and muscle maximal isometric force. The initial nominal parameters are repeatedly refined, as part of a least-squares optimization procedure, so that the mismatch between EMG-driven model's predicted prosthesis DOF commands and those applied to the prosthesis (predefined normalized velocities) is minimized. Calibration operates offline using prerecorded data. This enables calibration of both uni-lateral and bi-lateral amputees, since the subject mirrors the movement of the prosthesis with the phantom limb (instead of mirroring the contralateral healthy limb as in [20]).

System Communication Framework

The whole real-time modeling framework (i.e. EMG-driven Model and Calibration, Figs 1-2) operated on a laptop with dual-core processing unit (2.60GHz) and 16GB of RAM memory. Based on our recent work [24] we developed two software plug-in modules that enabled direct TCP/IP connection between the real-time modeling framework and external devices. The first plug-in module provided a direct TCP/IP connection to the external EMG amplifier. It recorded the raw EMGs and processed them as described in the Data Recording and Processing Section. The second plug-in module enabled a direct TCP/IP connection to the prosthetic limb. It processed the EMG-driven model-based estimates of wrist-hand moments to produce prosthesis low-level control commands, i.e. see Prosthesis Low-Level Controller Section.

Table II. Description of subjects investigated. Intact-limbed subjects are labeled as IL1-3. The transradial amputee individual is labeled as TR1.

	Age (Years)	Weight (Kg)	Height (cm)	Sex	Number of electrodes used	Amputation Level	Years since amputation	Prosthesis use
IL1	34	68	183	Male	8	-	-	-
IL2	26	73	177	Male	8	-	-	-
IL3	40	73	176	Male	8	-	-	-
TR1	50	75	168	Male	8	Transradial	30	Daily

Experimental Tests

Experiments were conducted in accordance with the declaration of Helsinki. The University Medical Center

Göttingen Ethical Committee approved all experimental procedures (Ethikkommission der

Universitätsmedizin Göttingen, approval number 22/4/16). Three intact-limbed individuals (IL1-3) and one transradial amputee (TR1, Table II) volunteered for this investigation after providing signed informed consent form. Amputation in the TR1 individual was a result of a traumatic injury at year 20th (Table II). Residual stump was estimated to be of 15 cm as measured from the stump most distal point to elbow lateral epicondyle. The TR1 individual is a regular prosthetic user currently fitted with a myocontrolled prosthesis (Michelangelo Hand, OttoBock HealthCare, GmbH) and the two-EMG-channel direct control scheme also used in our tests. None of the subjects had any neuromuscular disorder or abnormality than listed. Subjects performed three series of tasks including: virtual target reaching, clothespin, and functional tests. All tests were performed with no force feedback provided to the amputee.

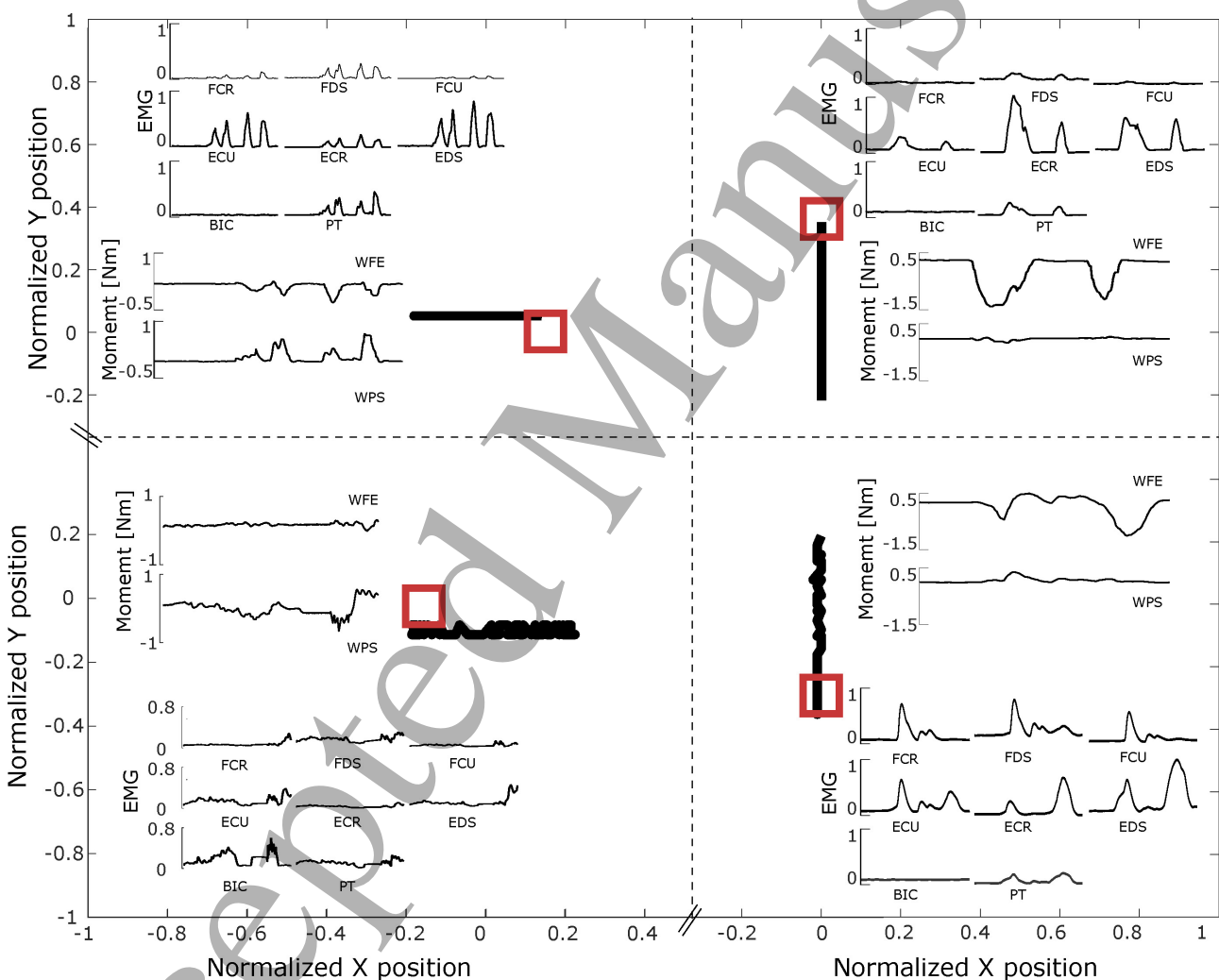
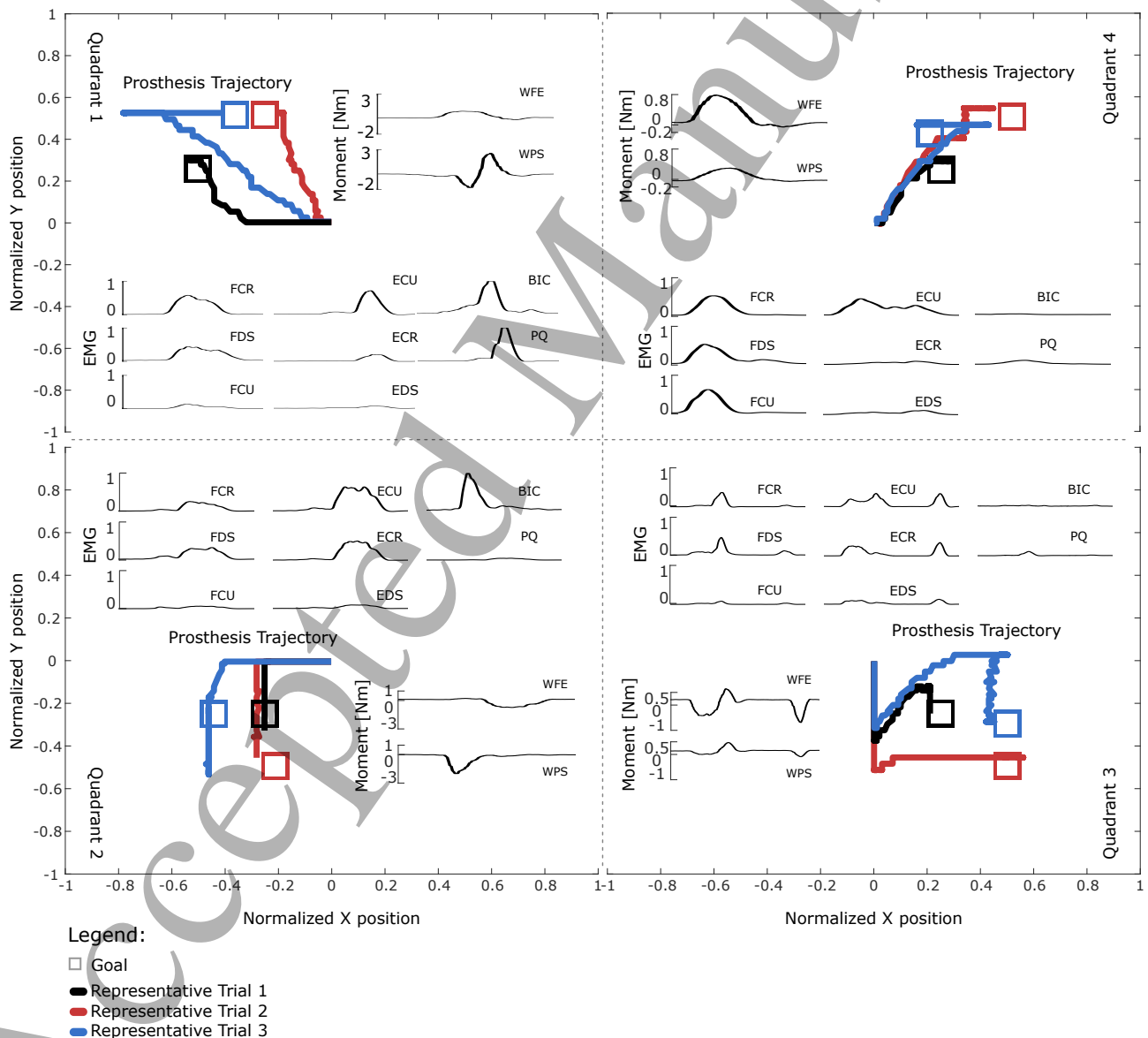


Figure 3. Vertical and horizontal target reaching tests reported for the transradial amputee (TR1).
 Four representative target positions to reach are depicted as red square-shaped cursors. The target workspace spanned the interval [-1, 1] in normalized units in both vertical and horizontal directions, where -1 and 1 corresponded to full pronation/flexion and supination/extension of the prosthesis. Vertical targets are

1
2 283 accomplished by operating the prosthesis wrist flexion-extension (WFE) degree of freedom (DOF).
3
4 284 Horizontal targets are accomplished by operating prosthesis forearm pronation-supination (WPS) DOF. Each
5
6 285 target is represented along with the underlying electromyograms (EMGs) recorded from the residual forearm
7
8 286 muscles including: flexor/extensor carpi radialis (FCR/ECR), flexor/extensor carpi ulnaris (FCU/ECU),
9
10 287 flexor/extensor digitorum superficialis (FDS/EDS), pronator teres (PT), and biceps brachii (BIC).
11
12 288 Furthermore, the resulting DOF moments predicted at the phantom limb WFE and WPS DOFs are depicted,
13
14 289 i.e. see black curves in each quadrant. EMGs are depicted as dimensionless curves whereas moments are
15
16 290 represented in Nm.
17
18 291
19
20 292



1
2 294 **Figure 4. Diagonal target reaching tests reported for the transradial amputee (TR1).** Results are
3 reported for each of the four quadrants. See Movie 1 for a visual example of quadrant 3 reaching tasks. Three
4 295 representative targets per quadrant are depicted as square-shaped cursors. Each target is reached from the
5 296 same initial position, i.e. zero degrees of wrist flexion and forearm pronation (hand neutral position). The
6 297 target workspace spanned the interval [-1, 1] in normalized units in vertical and horizontal directions, where
7 298 -1 and 1 corresponded to full pronation/flexion and supination/extension of the prosthesis. Each target is
8 299 reached by the simultaneous control of two degrees of freedoms (DOFs). In each quadrant, each target is
9 300 represented along with the underlying electromyograms (EMGs) recorded from the residual forearm muscles
10 301 including: flexor/extensor carpi radialis (FCR/ECR), flexor/extensor carpi ulnaris (FCU/ECU),
11 302 flexor/extensor digitorum superficialis (FDS/EDS), pronator teres (PT), and biceps brachii (BIC).
12 303 Furthermore, the resulting DOF moments predicted at the phantom limb wrist flexion-extension (WFE) and
13 304 forearm pronation-supination (WPS) DOFs are depicted, i.e. see black curves in each quadrant. Across all
14 305 quadrants and targets, vertical and horizontal directions are achieved by controlling WFE and WPS
15 306 respectively. EMGs are depicted as dimensionless curves whereas moments (torques) are represented in Nm.
16 307
17 308
18 309

Virtual Target Reaching Tasks

19 310 During the **virtual target reaching tasks**, subjects sat in front of a monitor and were asked to position
20 311 themselves on the chair so that their right arm could move freely in any direction. The monitor provided
21 312 visual feedback in the form of a ball-shaped cursor representing the prosthesis wrist flexion-extension and
22 313 pronation-supination kinematics state. Subjects were instructed to move a ball-shaped cursor to reach a
23 314 square-shaped target while keeping the cursor within the target for more than 1 second. Both cursor and
24 315 target moved in a Cartesian space. Cursor vertical movements were accomplished by actuating the prosthesis
25 316 wrist flexion-extension DOF via appropriate muscle contractions. Flexion and extension moved the cursor in
26 317 the negative and positive vertical directions respectively. Similarly, cursor horizontal movements were
27 318 accomplished by actuating the prosthesis wrist pronation-supination DOF. Pronation and supinations moved
28 319 the cursor in the negative and positive horizontal directions respectively. Prosthesis neutral position
29 320 corresponded to the cursor being in the Cartesian space origin. During all tasks, the myoelectric prosthesis
30 321 was located next to the subject.

1
2 322 The workspace spanned the interval [-1, 1] in normalized units in vertical and horizontal directions,
3
4 323 where -1 and 1 corresponded to full pronation/flexion and supination/extension of the prosthesis. The
5
6 324 prosthesis wrist range of motion was [-150, 150] and [-75, 50] degrees for pronation/supination and
7
8 325 flexion/extension respectively. Tasks were conducted with variable travel distance that ranged between 0.35
9
10 326 and 0.7 normalized units and with constant target size of 0.2 by 0.2 normalized units. The targets were
11
12 327 centered at the coordinates ($\pm 0.25, \pm 0.25$), ($\pm 0.25, \pm 0.5$), ($\pm 0.5, \pm 0.25$), and ($\pm 0.5, \pm 0.5$), where the signs of
13
14 328 the coordinates were determined by the quadrant that was tested. Subject performed two series of tests.
15
16
17 329 The first test series verified the system robustness to hand movement artefacts. Subjects were required to
18
19 330 repeatedly open and close their right biological or phantom hands in time to an acoustic metronomic cue, i.e.
20
21 331 50 beats per seconds, 10 repeated hand opening and closings. The subjects were instructed to exert 10 % of
22
23 332 their maximum opening\closing force.
24

25 333 The second test series verified the system ability to enable controlling WFE and WPS individually,
26
27 334 sequentially, as well as simultaneously. Subjects were required to perform a number of reaching tests. Each
28
29 335 test required reaching eight targets randomly located on the:
30
31
32 336 • Vertical axis only, i.e. prosthesis WFE DOF myoelectric control.
33
34 337 • Horizontal axis only, i.e. prosthesis WPS DOF myoelectric control.
35
36 338 • Cartesian space four quadrants using sequential control of prosthesis WFE and WPS DOFs.
37
38 339 • Cartesian space four quadrants respectively, i.e. top-left, bottom-left, top-right, bottom-right. Each
39
40 340 quadrant required the simultaneous and proportional control of the prosthesis WFE and WPS DOFs.
41

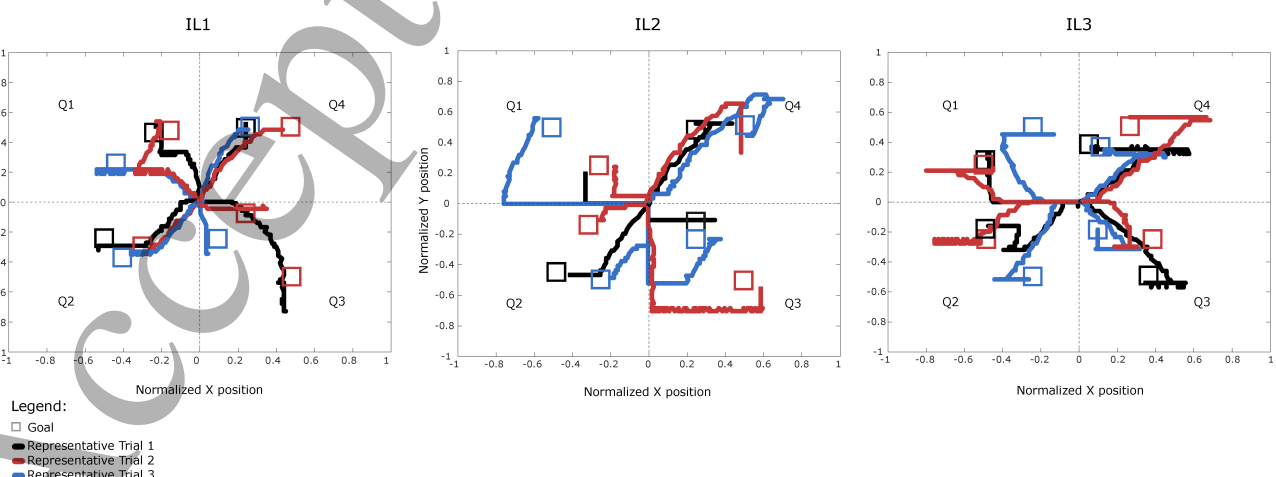
42 341 Importantly, in all the tests, the subjects could activate the DOFs simultaneously, but during horizontal,
43
44 342 vertical and sequential task, they were instructed to use a single DOF at a time. The aim of these tests was to
45
46 343 assess the selectivity of control and the amount of cross talk between the command signals (unwanted
47
48 344 activation). Each test series was repeated with the right arm in three different postures including: fully
49
50 345 extended elbow, 90 degree flexed elbow, 90 degree flexed elbow and 90 degree abducted shoulder. Arm
51
52 346 postures were monitored via inertial measurement units (XSens, Enschede, Netherlands) placed in the
53
54 347 correspondence of anatomical landmarks including: right acromion, humerus lateral compartment, forearm
55
56 348 lateral compartment. Moreover, each test was performed both using our proposed model-based system as
57
58
59
60

1
2 349 well as the classic commercial control system. The aim was to compare the performance of the novel method
3
4 350 to that of the commercial benchmark.
5
6 351
7
8 352

Clothespin Task

10 353 During the **clothespin task** subjects wore the prosthesis, which was connected to their forearms. For the
11 354 able-bodied subjects, the prosthesis was connected to a custom-made splint, which was then strapped to the
12 355 forearm. For the amputee subject, the prosthesis was mounted to a custom-made socket (as in a real-life
13 356 application). They stood in front of a clothespin test preparation platform. These tasks verified the ability to
14 355 accurately control WPS and HOC simultaneously and proportionally during functionally relevant tasks. Each
15 356 test was performed both using our proposed model-based system as well as the classic commercial control
16 357 system. Subjects performed two series of tests. The first test series involved grasping 12 pins located on
17 356 horizontal bars and placing them onto a vertical bar. Each pin triplet underlay different stiffness, hence the
18 357 need for grips with different force levels. This test was designed so that the subject needed to activate WPS
19 358 as well as HOC proportionally (to modulate force) and simultaneously (to activate multiple DOFs).
20
21 359

31 363 The second test series was a variation of the first. It involved performing a clothespin task with pins
32 364 equipped with custom-made contact sensor and an LED. When the pin fully closed, the sensor activated the
33 365 LED indicating that the exerted grasping force was too high, thereby “breaking” the “object”. The goal is to
34 366 grasp five pins each of which of different stiffness while accurately fine-tuning the grip force in order to
35 367 always keep it below a predefined threshold. More specifically, the subjects needed to exert enough force to
36 368 open the pin and remove it from the bar, but at the same time, the force had to be below the “breaking”
37 369 threshold of the pin. Therefore, each pin corresponded to a target window of grasping force.
38
39
40
41
42
43
44
45



1
2 371 **Figure 5. Diagonal target reaching tests reported for three intact-limbed individuals (IL1-3).** Three
3
4 372 representative targets per quadrant (Q1-Q4) are depicted as square-shaped cursors. Each target is reached
5
6 373 from the same initial position, i.e. zero degrees of wrist flexion and forearm pronation (hand neutral
7
8 374 position). The target workspace spanned the interval [-1, 1] in normalized units in vertical and horizontal
9
10 375 directions, where -1 and 1 corresponded to full pronation/flexion and supination/extension of the prosthesis.
11
12 376 Each target is reached by the simultaneous control of two degrees of freedoms (DOFs). Across all quadrants
13
14 377 and targets, vertical and horizontal directions are achieved by controlling WFE and WPS respectively. Also
15
16 378 see Movie 1 for a visual example of Q3 reaching tasks.

18
19 379
20
21 380 **Functional Tasks**
22

23 381 During the **functional tasks**, each subject wore the prosthesis and stood in front of a shelf. These tasks
24
25 382 verified the system ability of performing real-world functions robustly and intuitively. The tasks were
26
27 383 performed solely by using our proposed model-based system. Subjects performed three testing series. The
28
29 384 first was a block-turn task [43] involving a sequence of fine control actions including: grasping a narrow
30
31 385 wooden block placed on a high shelf, rotating it of 90 degrees, placing it back on the shelf, re-grasping the
32
33 386 block, rotating it back of 90 degrees, and replacing the block back to its initial position.

35
36 387 The second involved grasping a variety of objects ranging from small size and weight to large size and
37
38 388 weight: including an egg and a big bottle (1.5L). This investigated the system robustness in handling heavy
39
40 389 objects or preserving precise grip forces while handling delicate objects (i.e. eggs).

41
42 390 The third assessed the robustness of the system to EMG movement artefacts. It involved mechanical
43
44 391 perturbation in the EMG wired system to induce cable movement. This assessed whether the prosthesis
45
46 392 would be inadvertently activated (by movement-induced noise) and whether the user could still actively
47
48 393 control the prosthesis during the high noise condition.

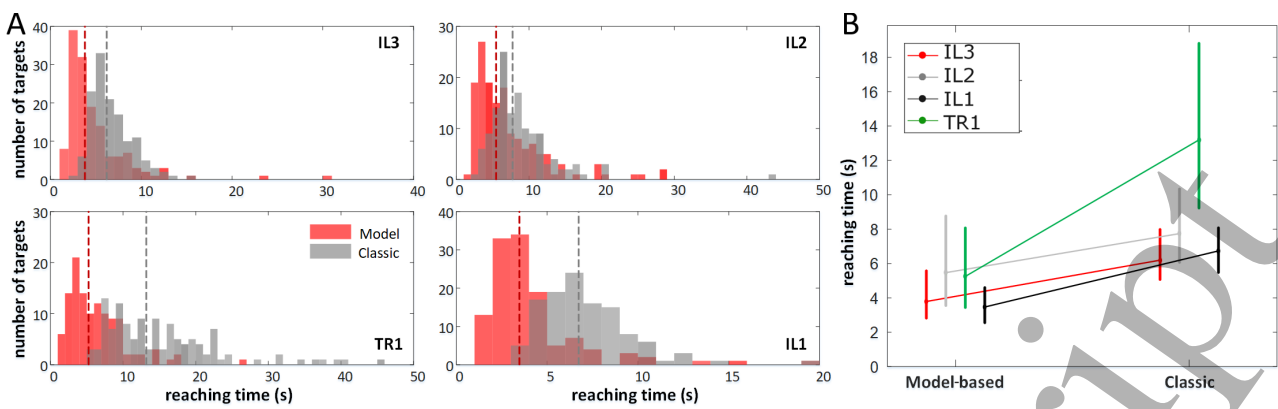


Figure 6. Speed performance during diagonal target reaching test reported for the transradial amputee (TR1) and for the three intact-limbed individuals (IL1-3). (A) Histograms report the distribution of reaching time across all targets for each subject individually, i.e. TR1 and IL1-3. Vertical dotted lines represent median reaching time. **(B)** Graphs report median (ball marker) and interquartile range (vertical line) of the time took to reach all targets as reported on a subject-specific basis. Targets in each quadrant and condition were accomplished both using our proposed model-based approach (model) as well as the classic commercially available system (classic).

Numerical Analysis

We quantified our proposed model-based framework real-time computation performance using metrics including: the mean computation time, standard deviation, median and 1st-3rd interquartile range measured across all simulation frames from all subjects and tasks. The 90% confidence interval was estimated for our proposed framework computation time using the Chebyshev's theorem, i.e., expected interval = mean \pm 3.16 · std. This could be applied with no assumption on the normality of computation time distributions. Path similarity between reaching trajectory and shortest path was calculated using the coefficient of determination (R^2 , square of the Pearson product moment correlation coefficient). In all the reaching tasks, we have determined the mean and standard deviation for the time to reach the target. The outcome measure in the clothespin task was the number of pins transferred per minute.

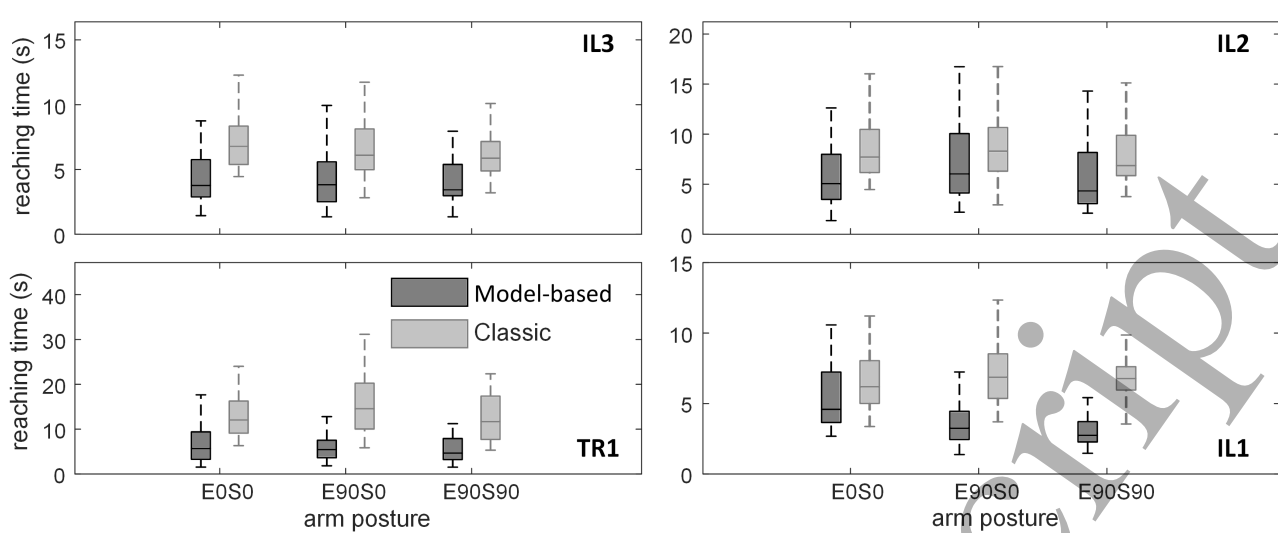


Figure 7. Speed performance as a function of arm position reported for the transradial amputee (TR1) and for the three intact-limbed individuals (IL1-3). Graphs report median (horizontal line), interquartile range (box), and overall max/min values (vertical dotted lines) of the time took to reach diagonal targets as a function of arm configurations: elbow/shoulder 0 degrees (E0S0), elbow 90 degrees flexed, shoulder 0 degrees (E90S0), elbow 90 degrees flexed, shoulder 90 deg abducted with hand closed (E90S90). Targets in each quadrant and condition were accomplished both using our proposed model-based approach (model-based) as well as the classic commercially available system (classic).

RESULTS

Our proposed real-time musculoskeletal model successfully converted EMG signals from eight forearm muscle groups into mechanical forces produced by 12 musculotendon units or MTUs (Table I) and into resulting EMG-dependent joint moments across a large repertoire of wrist-hand movement (Fig. 1A). EMG-driven model-based joint moment estimates were translated into prosthesis control commands (Fig. 1B), which resulted in the prosthesis moving naturally with no need for explicit angular position control. The prosthesis movement emerging from these commands was directly used to update the kinematic-dependent state in the musculoskeletal model (Fig 1C).

Results showed that our proposed paradigm enabled accurate and robust control of prosthesis WFE and WPS across a large repertoire of tasks performed at different arm configurations (Figs 3-7, Movie 1). Moreover, results showed the ability of natural control of WPS and HOC during functionally relevant clothespin tests (Figs 8, Movies 2-3) and object manipulation tests (Movies 4-7). These tests underwent

dynamic stump-prosthesis movements, enabling testing robustness to EMG non-stationarities (due relative movement between muscle fiber and electrodes) and control precision in the force domain. For all subjects, model calibration (Fig. 2) was always performed a number of days prior to real-time prosthesis control experiments. This provided evidence of the framework ability of retaining subject-specific parameter consistency across time scales, i.e. the model needed to be established once for all per subject. Subjects controlled the prosthesis throughout three series of tasks including: virtual target reaching, clothespin, and functional tasks. This Section presents quantitative results as well as the framework computational times across all series of tasks. In the reminder of this section the three intact-limbed individuals will be referred to as IL1, IL2, and IL3 respectively. The transradial amputee will be referred to as TR1 as indicated in Table II.

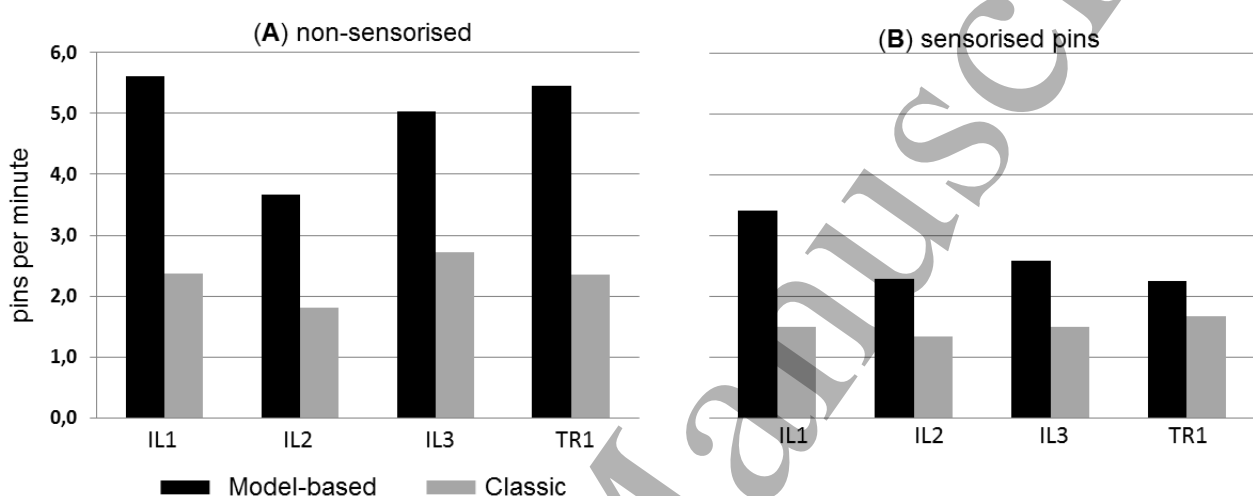
Virtual Target Reaching Tasks

The virtual target reaching tasks tested whether the proposed framework enabled subjects to control prosthesis WFE and WPS individually, sequentially, as well as simultaneously. Subjects sat in front of a monitor and were instructed to move a virtual ball-shaped cursor to reach a square-shaped target and keep the cursor within the target for ~1 second. Cursor movements were accomplished by actuating prosthesis WFE and WPS DOFs via forearm muscle contractions. Since it is known that arm posture greatly affects the performance of state of the art decoders [2], we quantified our system robustness to arm configuration, i.e. each test was repeated with the right arm in three postures: (a) fully extended elbow, (b) 90-degree flexed elbow, and (c) 90-degree flexed elbow and 90-degree abducted shoulder.

During the virtual target reaching tasks subjects reached a total of 672 targets, i.e. 168 targets per subjects on average. The first three series of tests verified the precision in controlling WFE and WPS individually (i.e. first and second series, see Methods Section) as well as sequentially (i.e. third series, see Methods Section) in order to reach vertically and/or horizontally displayed targets. Importantly, in all three series, the system always allowed simultaneous DOF control, but subjects were instructed to activate the DOFs individually, testing thereby the ability for selective control. Fig. 3 depicts vertical and horizontal reaching trajectories (i.e. individual DOF control) reported for TR1 along with recorded EMGs and estimated WFE and WPS moments driving the prosthesis movement. Subjects always reached targets using linear trajectories thereby successfully actuating a single DOF at a time with high precision. Path similarity was always accomplished with $R^2 > 0.98$ across all targets and subjects. Intact-limbed individuals and transradial

1
2 463 amputee reached all targets with comparable times (median\interquartile range) during the individual and
3 sequential DOF (two DOFs controlled in sequence) control tasks: 2.2\1.6s (individual) and 4.6\3.1s
4 464 (sequential) across IL1-3 whereas 2.3\1.6s (individual) and 7.1\5.1s (sequential) for TR1.
5
6 465
7
8 466
9 The fourth series of tests verified the system ability to enable controlling WFE and WPS simultaneously.
10 467 Movie 1 shows the proposed model-based framework operated in real-time for the control of the prosthesis
11 by IL1, displaying both musculoskeletal model, recorded EMGs and estimated wrist moments. The movie
12 468 also shows the concurrent control of the ball-shaped cursor for reaching a variety of diagonal targets (see
13
14 469 user interface on external screen). Note that the cursor diagonal trajectories directly correspond to the
15
16 470 prosthesis simultaneous actuation of WPS and WFE. Fig. 4 further depicts diagonal reaching trajectories
17
18 471 reported for TR1 along with recorded EMGs and estimated WFE and WPS moments driving the prosthesis
19
20 472 movement. Fig. 4 shows highly coupled production of WFE and WPS moments underlying simultaneous
21
22 473 control of prosthesis DOFs. Moment generating patterns were substantially different during the sequential
23
24 474 DOF tasks (Fig. 3), i.e. reduced degree of WFE and WPS moment coupling. Fig. 5 depicts representative
25
26 475 diagonal reaching trajectories for all intact-limbed individuals. Figs 4 and 5 also show that all subjects were
27
28 476 able to produce diagonal trajectories. Moreover, each individual displayed ability of generating optimal
29
30 477 diagonal trajectories in specific quadrants. TR1 was particularly capable of generating diagonal trajectories
31
32 478 in quadrants 1, 3 and 4. IL1 and IL3 were capable of generating diagonal trajectories across all quadrants
33
34 479 whereas IL2 in quadrants 2 and 4.
35
36 480
37
38 481 Intact-limbed individuals and transradial amputee reached all targets with comparable times
39
40 482 (median\interquartile range), i.e. 3.8\2.8s across IL1-3 and 5.3\4.7s for TR1. Each individual reached targets
41
42 483 with substantially less time using our proposed model-based framework (model-based) than when using the
43
44 484 classic commercially available two-channel sequential control scheme based on co-contraction (classic). Figs
45
46 485 6A and 6B respectively reports the distribution and median\interquartile range of reaching times across all
47
48 486 targets on a subject-specific basis. Across all subjects, quadrant 1 targets were reached (median\interquartile
49
50 487 range) in 3.4\2.9s (model-based) and 6.2\3.4s (classic). Quadrant 2 targets were reached in 4.1\3.4s (model-
51
52 488 based) and 5.9\2.6s (classic). Quadrant 3 targets were reached in 3.4\2.2s (model-based) and 7.4\3.7s
53
54 489 (classic). Quadrant 4 targets were reached in 4.2\3.9s (model-based) and 5.8\2.4s (classic).
55
56
57 490 Importantly, the performance of the proposed model-based approach was preserved across all arm
58
59 491 postures. Fig. 7 reports reaching times across arm postures and specifically for each subject. This shows our

1
2 492 proposed model-based approach has no performance decay across arm configuration and consistently
3
4 493 outperforms the robust classic control scheme. In this, reaching times were always smaller using the model-
5
6 494 based approach than when using the classic control scheme. Across all subjects, reaching times during
7
8 495 extended elbow posture were (median\interquartile range) 3.1\2.2s (model-based) and 7.1\3.8s (classic).
9
10 496 During elbow flexed arm posture they were 3.4\3s (model-based) and 6.2\4.9s (classic). Finally, during
11
12 497 elbow flexed and shoulder abducted arm posture they were 3.3\2s (model-based) and 5.9\3.7s (classic).
13
14 498



31 499
32
33 500 **Figure 8. Speed performance during clothespin test.** Performance is evaluated in terms of number of
34 501 clothespins correctly picked and placed per minute (ppm) both using our proposed system (model-based) and
35 502 the commercially available system (classic). Results are reported for three intact-limbed individuals (IL1-3)
36 503 and one transradial amputee (TR1). Also refer to Table II. (A) Results are reported for the non-sensorised pin
37 504 test. (B) Performance is evaluated in terms of number of sensorised clothespins correctly picked without
38 505 triggering light sensor.
39
40
41
42
43
44
45
46
47
48
49

Clothespin Task

50 506
51 507 The clothespin task verified the ability to accurately control WPS and HOC simultaneously and
52 508 proportionally across functionally relevant tasks. Subjects performed two series of tests with different pin
53 509 types. Subjects picked a total of 48 non-sensorised pins (i.e. 12 pins per subject) and a total of 20 sensorized
54 510 pins (i.e. 5 pins per subject).
55
56
57
58

59 511 The first series of tests (Movie 2, Fig. 8A) involved picking and placing non-sensorised pins (see
60 512 Methods Section). Pins were arranged in four triplets of different stiffness as previously reported [44].
513

1
2 514 Results showed that both intact-limbed and amputee individuals could control prosthesis WPS and HOC
3
4 515 simultaneously while generating natural motions. This enabled individuals to complete the test with an
5
6 516 average speed of 5.24 ± 0.9 pins per minute (ppm) using the proposed model-based framework. In this, the
7
8 517 amputee's speed performance (5.5 ± 0.4 ppm) was comparable to that of subject IL1 (5.6 ± 0.7 ppm) and higher
9
10 518 than that of subjects IL2 (3.67 ± 0.5 ppm) and IL3 (5.03 ± 0.6 ppm). Each individual completed the test with
11
12 519 substantially better performance than when they used the commercially available sequential control scheme
13
14 520 based on co-contraction (Fig. 8A) [9]. For the classic-control scheme, average speed performance was
15
16 521 2.3 ± 0.4 ppm and ranged between 1.8 ± 0.1 ppm (subject IL2) and 2.7 ± 0.2 ppm (subject IL3).

18
19 522 The second series (Movie 3, Fig. 8B) involved picking and placing sensorised pins equipped with
20
21 523 custom-made contact sensors. The sensor registered when the pin was grasped with force levels beyond
22
23 524 predefined thresholds. This was indicated by activating a LED signaling that the subject would have
24
25 525 "broken" the grasped object in the real world. Similarly to the first series, test underlay five pins of different
26
27 526 stiffness as previously reported (see Material and Methods Section) [44]. The aim was to pick each pin while
28
29 527 accurately controlling grasping force in order to open the pin enough to remove it from the bar but without
30
31 528 using excessive forces, which would trigger the light sensor. The target force windows to successfully
32
33 529 relocate each pin were 7-15% (yellow pins in Movies 2-3), 13-23% (red pins in Movies 2-3), 23-32% (green
34
35 530 pins in Movies 2-3), and 35-43% (black pins in Movies 2-3) of the prosthesis maximum force. Results
36
37 531 revealed each individual's ability of fine controlling the prosthesis grip force while simultaneously
38
39 532 controlling hand rotation. Movie 3 shows the amputee's ability of grasping sensorized pins with the
40
41 533 appropriate force level while preserving the required force level accurately during prosthesis wrist pronation-
42
43 534 supination, hence with no unwanted activations, i.e. no cross talk across DOFs. Individuals completed the
44
45 535 sensorized clothespin test with an average speed of 2.7 ± 0.4 pins per minute (ppm) using the proposed model-
46
47 536 based framework (Fig. 9). In this, the amputee's speed performance (2.25 ± 0.1 ppm) was comparable to that
48
49 537 of intact-limbed subject IL2 (2.28 ± 0.2 ppm) IL3 (2.58 ± 0.2 ppm) while IL1 (3.4 ± 0.2 ppm) displayed the best
50
51 538 performance. Similarly to the first test, each individual completed the test with better performance than when
52
53 539 they used the commercially available sequential control scheme based on co-contraction (Fig. 9) [9]. For the
54
55 540 classic-control scheme, average speed performance was 1.5 ± 0.13 ppm and ranged between 1.3 ppm (subject
56
57 541 IL2) and 1.6 ppm (subject TR1).

Functional Tasks

The functional tasks verified the system ability of performing real-world functions robustly and intuitively and were performed only with the proposed model-based control scheme. Results are reported in the form of a large repertoire of videos. In this, the transradial amputee could successfully perform tasks involving fine control actions (Movies 4-5) as well as manipulation of different objects (Movies 6-7). Fine control actions are displayed in Movie 4, showing TR1 executing a block-turn task involving fine control of HOC and WPS DOFs in the precise positioning of a narrow wooden block in equilibrium on a wooden shelf. Movie 5 shows TR1 precisely controlling HOC DOF force for grasping an egg. The movie shows TR1 ability of grasping force fine control while rotating the prosthetic wrist without breaking the egg. It is worth stressing that this task was performed with no force feedback provided to the amputee. Movie 7 shows how our proposed system was transparent to mechanically induced EMG movement artefacts, preventing inadvertently activating the prosthesis DOFs, i.e. by the resulting noise. Remarkably, the proposed system always enabled amputee's voluntary prosthesis control under high movement-artefact contaminated condition. Finally, the system proved to be robust to highly dynamic movements including grasping and manipulating heavy objects (i.e. a 1.5L water bottle, Movie 7), a tasks that would be challenging for state of the art non-invasive myoelectric systems due to underlying alterations in EMG patterns in response to object weight [2,9,11].

Computational Time

Across all subjects and tests the proposed framework generated prosthesis control commands with average speeds 35 ± 11 ms. This includes the total net delay from the EMG recording to final prosthesis actuation. In this, 90% of control commands produced in one single time frame were generated within 55ms. This is well within the human perceivable delay in motor execution [45,46].

DISCUSSION

We presented a paradigm of man-machine interfacing where the complete information extracted from an individual's composite neuromusculoskeletal system (i.e. from neuromuscular activation to skeletal joint mechanics) is used to control a robotic multi-functional prosthetic limb. We tested this paradigm on three intact-limbed individuals and on one transradial amputee during a range of tasks involving real-time control

1
2 571 of a physical prosthesis. The results showed performance and control capabilities superior than state of the
3 art non-invasive myocontrol approaches.
4
5

6 573 Our proposed neuro-mechanical interface addressed a major limit in current state of the art decoders, i.e.
7
8 574 the inability of synthetizing the mechanisms that the neuro-musculo-skeletal system uses to control
9 biological joints. State of the art consolidated approaches to the control of artificial limbs are based on
10 575 machine learning for establishing a single mapping function between EMG and joint kinematics. In this
11
12 576 context, there currently exist commercial systems based on pattern recognition (e.g. Coapt LLC) that showed
13
14 577 important clinical use [47,48]. Moreover, recent regression based methods have shown levels of robustness
15
16 578 to noise [49]. However, current machine learning approaches still display sensitivity to electrode
17
18 579 replacement as well as lack of robustness to arm postures, thus providing control paradigms that are sensitive
19
20 580 to external conditions.
21
22
23 581
24

25 582 We propose an alternative idea based on a biomimetic model-based decoder, i.e. a computational model
26
27 583 that explicitly synthesizes the dynamics of the musculo-skeletal system as controlled by neural surrogates,
28
29 584 i.e. EMG-derived muscle activation signals (Fig. 1). Although online modelling was previously employed in
30
31 585 lower limb prostheses [50] and robotic exoskeleton [51,52] scenarios, our study proposes a paradigm never
32
33 586 presented for online myoelectric prosthesis control in transradial amputees. Forearm EMG recordings are
34
35 587 used to drive forward physiologically correct models of the human musculoskeletal system in real-time,
36
37 588 rather than regressing “all the way to” joint angles. This provides a completely new approach to decode
38
39 589 amputees’ phantom limb function and concurrently control upper limb prostheses. This model-based
40
41 590 biomimetic approach enabled for the first time decoding a transradial amputee’s phantom limb mechanical
42
43 591 moments (Figs 3-4) and concurrently mimicking biological wrist function in artificial limbs in real-time
44
45 592 (Movies 1-7). Whether joint moments could be reliably decoded from an amputee’s residual muscles EMG
46
47 593 to robustly control a prosthetic wrist-hand represented an unanswered scientific question that this work
48
49 594 directly addressed. In our paradigm, the prosthesis is the physical device that converted EMG-predicted joint
50
51 595 moments into joint angles, thus eliminating the need for numerically integrating dynamic equations of
52
53 596 motions. This is different from current solutions operating at the kinematic-level, including (1) model-free
54
55 597 decoders, sensitive to unseen motor tasks and time scales [5] and model-based methods [21] that integrate
56
57 598 forward dynamic equations of motion, which is a computationally expansive and numerically unstable step
58
59 599 [23].

1
2 600 Removing the need for integrating the equation of motion is central for simulating large-scale models, an
3 important element especially relevant for individuals who underwent targeted muscle reinnervation surgical
4 procedures, who require regaining control of large sets of skeletal DOFs. Our proposed biomimetic model-
5 based approach enables control intuitiveness. In this, subjects do not have to learn to produce a specific
6 EMG pattern for prosthesis control. They only need to move their own biological or phantom limb, whose
7 mechanical function is directly captured by the neuro-mechanical interface and concurrently rendered in the
8 real-world by the controlled prosthetic limb.
9
10 604
11 605
12 606
13 607
14 608
15 609
16 610
17 611
18 612
19 613
20 614
21 615
22 616
23 617
24 618
25 619
26 620
27 621
28 622
29 623
30 624
31 625
32 626
33 627
34 628

Results have demonstrated that our method provided an advanced and reliable prosthesis control across tests involving reaching ~600 virtual targets from three arm postures, manipulation of 48 non-sensorised clothespins, 20 sensorised clothespins as well as manipulation of real-world objects during tasks mimicking daily living scenarios. The subjects could successfully activate prosthesis DOFs simultaneously (WFS and WPS, WPS and HOC) across a large range of tasks, and they could proportionally modulate the ratio of the DOF activations, as demonstrated by the diagonal trajectories with different slopes in Figs 4-5. Furthermore, subjects successfully activated single DOFs and transitioned between DOFs sequentially, with minimal cross talk between DOF-specific command signals, which has shown to be a challenge for regression-based methods [53]. Our method consistently and significantly outperformed commercially available benchmark systems (i.e. robust two channel command interface, commercial benchmark) during multi-DOF tasks but also during single-DOF tasks where commercial benchmarks would be expected to best perform. This was evident in the case of the amputee subject, an especially encouraging result.

Fig. 3 shows that in some cases, subjects did not reach a given target via a single muscle contraction but rather via a sequence of brief contractions. This resulted in a number of trajectories underling a sequence torque pulses, dictating virtual cursor movement along a straight path with a variable velocity. Future work will assess whether practice will enable subjects to minimize the number of contractions needed to reach a give target. Fig. 4, shows that certain DOF combinations were achieved via minimally overlapped moment curves. While this is in line with literature studies on natural wrist rotations [54–58], it may also be a consequence of the fact that certain DOF-combinations are more intuitive than others. This may be especially relevant for the amputee subject who performed the tasks with no visual feedback on the prosthesis (please see Movie 1). Future work will also assess to what extent the lack of intrinsic muscle EMGs may contribute to decoded joint moments across coordinated wrist-hand tasks.

1
2 629 Our proposed approach demonstrated decoding robustness across a large variety of wrist-hand tasks
3
4 630 (Movie 1) performed across different arm configurations (Figs. 6-7), and during dynamic tasks (i.e. Movies
5
6 631 4-7). Movie 6 demonstrated our system ability to generate no unwanted prosthesis movement when EMG
7
8 632 electrode cables underwent mechanically induced movement artefacts. Although this is not representative of
9 commercially available systems schemes (i.e. involving no external cables that could be perturbed), these
10 633 results show the potential robustness of our system to external movement artefact that may nevertheless
11 634 come from interaction with the environment. Moreover, it enabled performing highly dynamic motor tasks
12 635 including manipulating heavy objects (Movie 7).

18
19 637 Our system robustness (which was comparable to the most robust benchmark system in the market)
20
21 638 derived from the fact that any joint moment estimate must always exist within the musculoskeletal model
22
23 639 operational space and be therefore physiologically plausible. This cannot be achieved with current machine
24
25 640 learning decoders that, when trained in one condition, would produce unrealistic estimates (i.e. outside the
26
27 641 physiological space) in novel conditions. Machine learning decoding solutions are not constrained by any
28
29 642 physiologically plausible structure. Our proposed approach establishes a subject-specific model of an
30
31 643 individual's musculoskeletal system. In this, the musculoskeletal model linear scaling and parameter non-
32
33 644 linear calibration (i.e. see Methods Section, Fig. 2) directly determine how EMG signals are processed by the
34
35 645 subject's musculoskeletal system, i.e. how they are converted into muscle force and further projected onto
36
37 646 skeletal DOFs. This effectively reduces the space of potential solutions as EMGs can be mapped only onto
38
39 647 mechanical forces that are contained within the musculoskeletal model operational space. Current methods
40
41 648 map EMG signals into control commands with no physiological constraints, thus dealing with large solution
42
43 649 spaces that contain large portions of non-physiologically plausible solutions.

46 650 Results were obtained on a small number of subjects. Future work will be directed in testing the
47
48 651 generalization of the results to a greater population encompassing subjects with different levels of
49
50 652 amputations as well as comparison of our methodology with respect to state-of-the-art pattern recognition
51
52 653 techniques. Our proposed method demonstrated applicability in amputees who underwent traumatic injuries.
53
54 654 Future work will assess whether this method can be translated to individuals affected by congenital limb
55
56 655 absence. This will require a systematic research to investigate whether motor task learning can be induced in
57
58 656 such individuals undergoing physiotherapy training coupled with the proposed real-time system. Further
59
60 657 research is also needed to investigate to what extent Hill-type muscle models may contribute to reduce EMG

noise artefacts in online myocontrol scenarios. In this context, computational muscle models may enable simulating musculotendon viscoelasticity, which may act as a dynamic filter for reducing the impact of noise remaining in the EMG after linear envelope computation. Although our results provided evidence of robustness to arm configurations further work is necessary to assess robustness to other sources of noise. Future work will also perform systematic analyses to quantify to what extend the model scaling and calibration procedures (see Methods Section) can be retained for a subject across time scales, i.e. involving longitudinal testing over a number of consecutive weeks.

CONCLUSION

This study showed the potential of the proposed control method to enable the first real-time multi-DOF myoelectric technology that decodes an amputee's phantom limb musculoskeletal mechanics and could be employed in real-world scenarios to control a total of three DOFs including forearm pronation-supination, wrist flexion-extension and hand opening-closing. Future work will couple our proposed model-based approach with deconvolution-based decoding of motor neuron discharges from high-density electromyograms and enable bionic limb control in higher-dimensional DOF spaces [1,30]. Integrating model-based paradigms as a mechanism to constrain and control prosthetic wrist-hand rotation within physiologically plausible operational spaces has the potential to bring prosthetic technology closer to match biological joint function with implications for both upper and lower limb rehabilitation technologies. It will enable individuals to control artificial limbs by estimating physiological activations in their residual muscles, hence control intuitiveness. It will enable decoding "any" movement (i.e. not only those learned in a specific regime) because it synthesizes the underlying neuromuscular processes, hence control robustness and extrapolation to unseen conditions. It will enable predicting internal somatosensory variables (i.e. muscle/tendon length, tension), which will help restore amputees' somatosensory processes in advanced closed-loop neuro-prostheses.

REFERENCES

- [1] Farina D, Vujaklija I, Sartori M, Kapelner T, Negro F, Jiang N, Bergmeister K, Andalib A, Principe J and Aszmann O C 2017 Man/machine interface based on the discharge timings of spinal motor neurons after targeted muscle reinnervation *Nat. Biomed. Eng.* **1** 0025

- 1
2 687 [2] Farina D and Aszmann O 2014 Bionic Limbs: Clinical Reality and Academic Promises. *Sci. Transl.
3
4 688 Med.* **6** 257ps12
5
6 689 [3] Micera S, Rossini P M, Rigosa J, Citi L, Carpaneto J, Raspopovic S, Tombini M, Cipriani C,
7 Assenza G, Carrozza M C, Hoffmann K-P, Yoshida K, Navarro X and Dario P 2011 Decoding of
8 690 grasping information from neural signals recorded using peripheral intrafascicular interfaces. *J.
9
10 691 Neuroeng. Rehabil.* **8** 53
11
12 692 [4] Kuiken T A, Miller L A, Lipschutz R D, Lock B A, Stubblefield K, Marasco P D, Zhou P, Dumanian G
13
14 693 A, Stubblefield K, Marasco P D, Zhou P and Dumanian G A 2007 Targeted reinnervation for
15
16 enhanced prosthetic arm function in a woman with a proximal amputation: a case study. *Lancet* **369**
17
18 19695 371–80
20
21 21696 [5] Jiang N, Dosen S, Muller K R and Farina D 2012 Myoelectric Control of Artificial Limbs: Is There a
22
23 23697 Need to Change Focus? [In the Spotlight] *IEEE Signal Process. Mag.* **29** 150–2
24
25 25698 [6] Hahne J M, Bießmann F, Jiang N, Rehbaum H, Member S, Farina D, Member S, Meinecke F C,
26 Müller K and Parra L C 2014 Linear and Nonlinear Regression Techniques for Simultaneous and
27 27699 Proportional Myoelectric Control **22** 269–79
28
29 29700 [7] Farina D, Jiang N, Rehbaum H, Holobar A, Graimann B, Dietl H and Aszmann O C 2014 The
30
31 31701 extraction of neural information from the surface EMG for the control of upper-limb prostheses:
32
33 Emerging avenues and challenges *IEEE Trans. Neural Syst. Rehabil. Eng.* **22** 797–809
34
35 34702 [8] Enoka R M 2008 *Neuromechanics of Human Movement* (Human Kinetics Publishers, Inc.)
36
37 36703 [9] Jiang N, Dosen S, Muller K R and Farina D 2012 Myoelectric Control of Artificial Limbs: Is There a
38
39 Need to Change Focus? [In the Spotlight] *IEEE Signal Process. Mag.* **29** 150–2
40
41 40705 [10] Ifft P J, Shokur S, Li Z, Lebedev M a and Nicolelis M a L 2013 A brain-machine interface enables
42
43 bimanual arm movements in monkeys. *Sci. Transl. Med.* **5** 210ra154
44
45 46708 [11] Sartori M, Lloyd D G and Farina D 2016 Neural Data-driven Musculoskeletal Modeling for
46
47 Personalized Neurorehabilitation Technologies *IEEE Trans. Biomed. Eng.* **63** 879–93
48
49 48709 [12] Lloyd D G and Besier T F 2003 An EMG-driven musculoskeletal model to estimate muscle forces
50
51 and knee joint moments in vivo *J. Biomech.* **36** 765–76
52
53 52711 [13] Sartori M, Reggiani M, Farina D and Lloyd D G 2012 EMG-driven forward-dynamic estimation of
54
55 muscle force and joint moment about multiple degrees of freedom in the human lower extremity
56
57 57713
58
59 59714
60
61 61715

1
2 716 PLoS One **7** 1–11
3
4 717 [14] Sartori M, Farina D and Lloyd D G 2014 Hybrid neuromusculoskeletal modeling to best track joint
5 moments using a balance between muscle excitations derived from electromyograms and
6 718 optimization *J. Biomech.* **47** 3613–21
7
8 719
9
10 720 [15] Durandau G, Farina D and Sartori M 2018 Robust Real-Time Musculoskeletal Modeling driven by
11 Electromyograms *IEEE Trans. Biomed. Eng.* **65** 556–64
12 721
13
14 722 [16] Manal K, Gravare-Silbernagel K and Buchanan T S 2011 A real-time EMG-driven musculoskeletal
15 model of the ankle *Multibody Syst. Dyn.* **28** 169–80
16
17 723
18
19 724 [17] Pizzolato C, Reggiani M, Saxby D J, Ceseracciu E, Modenese L and Lloyd D G 2017 Biofeedback
20 for Gait Retraining Based on Real-Time Estimation of Tibiofemoral Joint Contact Forces *IEEE*
21
22
23 726 [18] Manal K, Gonzalez R V, Lloyd D G and Buchanan T S 2002 A real-time EMG-driven virtual arm.
24
25 727
26
27 728 [19] Chadwick E K, Blana D, van den Bogert A J T and Kirsch R F 2009 A real-time, 3-D
28
29 729 musculoskeletal model for dynamic simulation of arm movements. *IEEE Trans. Biomed. Eng.* **56**
30
31 730
32
33 731 [20] Crouch D L and He H 2016 Lumped-parameter electromyogram-driven musculoskeletal hand
34
35 model: A potential platform for real-time prosthesis control *J. Biomech.* **49** 3901–7
36 732
37
38 733 [21] Crouch D L and Huang H (Helen) 2017 Musculoskeletal model-based control interface mimics
39
40 734 physiologic hand dynamics during path tracing task *J. Neural Eng.* **14** 036008
41
42 735
43
44 736 [22] Pan L, Crouch D L and Huang H 2018 Myoelectric Control Based on a Generic Musculoskeletal
45
46 737 Model: Toward a Multi-User Neural-Machine Interface *IEEE Trans. Neural Syst. Rehabil. Eng.* **26**
47
48 738
49
50 739 [23] Blana D, Chadwick E K, van den Bogert A J and Murray W M 2017 Real-time simulation of hand
51 motion for prosthesis control *Comput. Methods Biomed. Engin.* **20** 540–9
52
53 740
54
55 741 [24] Durandau G, Farina D and Sartori M Real-time musculoskeletal modeling driven by
56
57 742 electromyograms *IEEE Trans. Biomed. Eng.*
58
59 743 [25] Schaffelhofer S, Sartori M, Scherberger H and Farina D 2015 Musculoskeletal Representation of a
60 Large Repertoire of Hand Grasping Actions in Primates *IEEE Trans. Neural Syst. Rehabil. Eng.* **23**

- 1
2 745 210–20
3
4 746 [26] Sartori M, Reggiani M, Pagello E and Lloyd D G 2012 Modeling the human knee for assistive
5 technologies. *IEEE Trans. Biomed. Eng.* **59** 2642–9
6 747
7
8 748 [27] Sartori M, Reggiani M, van den Bogert A J and Lloyd D G 2012 Estimation of musculotendon
9 kinematics in large musculoskeletal models using multidimensional B-splines *J. Biomech.* **45** 595–
10 749
11
12 750 601
13
14 751 [28] Sartori M, Maculan M, Pizzolato C, Reggiani M and Farina D 2015 Modeling and Simulating the
15 Neuromuscular Mechanisms regulating Ankle and Knee Joint Stiffness during Human Locomotion *J.
16
17 752
18
19 753 *Neurophysiol.* **114** 2509–27
20
21 754 [29] Sartori M, Lloyd D G and Farina D 2016 Neural data-driven musculoskeletal modeling for
22 personalized neurorehabilitation technologies *IEEE Trans. Biomed. Eng.* **63** 879–93
23
24
25 755 [30] Sartori M, Yavuz U S and Farina D 2017 In Vivo Neuromechanics: Decoding Causal Motor Neuron
26 Behavior with Resulting Musculoskeletal Function *Sci. Rep.* **7** 13465
27
28
29 756 [31] Besier T F, Lloyd D G and Ackland T R 2003 Muscle activation strategies at the knee during
30 running and cutting maneuvers. *Med. Sci. Sports Exerc.* **35** 119–27
31
32 757
33
34 758 [32] Manal K and Buchanan T S 2003 A one-parameter neural activation to muscle activation model:
35 estimating isometric joint moments from electromyograms. *J. Biomech.* **36** 1197–202
36
37
38 760 [33] Shao Q, Bassett D N, Manal K and Buchanan T S 2009 An EMG-driven Model to Estimate Muscle
39 Forces and Joint Moments in Stroke Patients *Comput. Biol. Med.* **39** 1083–8
40
41
42 764 [34] Higginson J S, Ramsay J W and Buchanan T S 2012 Hybrid models of the neuromusculoskeletal
43 system improve subject-specificity *Proc. Inst. Mech. Eng. Part H J. Eng. Med.* **226** 113–9
44
45
46 766 [35] Manal K and Buchanan T S 2005 Use of an EMG-driven biomechanical model to study virtual
47 injuries. *Med. Sci. Sports Exerc.* **37** 1917–23
48
49
50 768 [36] Barrett R, Besier T and Lloyd D 2007 Individual muscle contributions to the swing phase of gait: An
51 EMG-based forward dynamics modelling approach *Simul. Model. Pract. Theory* **15** 1146–55
52
53
54 770 [37] Hayashibe M and Guiraud D 2013 Voluntary EMG-to-force estimation with a multi-scale
55 physiological muscle model. *Biomed. Eng. Online* **12** 86
56
57
58 772 [38] Delp S L, Anderson F C, Arnold A S, Loan P, Habib A, John C T, Guendelman E and Thelen D G
59
60
61
62
63
64
65
66
67
68
69
70
71
72
73 2007 OpenSim: open-source software to create and analyze dynamic simulations of movement. *IEEE**

- 1
2 774 *Trans. Biomed. Eng.* **54** 1940–50
3
4 775 [39] Saul K R, Hu X, Goehler C M, Vidt M E, Daly M, Velisar A and Murray W M 2014 Benchmarking
5
6 776 of dynamic simulation predictions in two software platforms using an upper limb musculoskeletal
7
8 777 model. *Comput. Methods Biomech. Biomed. Engin.* 1–14
9
10 778 [40] H.J. Hermens and B Freriks 2017 SENIAM Project *SENIAM Proj.* 1
11
12 779 [41] Sartori M, Gizzi L, Lloyd D G D G and Farina D 2013 A musculoskeletal model of human
13
14 780 locomotion driven by a low dimensional set of impulsive excitation primitives *Front. Comput.*
15
16 781 *Neurosci.* **7** 79
17
18 782 [42] Sartori M, Maculan M, Pizzolato C, Reggiani M and Farina D 2015 A Theoretical and
20
21 783 Computational Framework for Modeling and Simulating Musculoskeletal Stiffness during
22
23 784 Locomotion *The 25th Congress of the International Society of Biomechanics* (Glasgow) pp 1–2
24
25 785 [43] Amsuess S, Vujaklija I, Gobel P, Roche A, Graumann B, Aszmann O and Farina D 2015 Context-
26
27 786 Dependent Upper Limb Prosthesis Control for Natural and Robust Use *IEEE Trans. Neural Syst.*
28
29 787 *Rehabil. Eng.* **43** 20 1–1
30
31 788 [44] De Nunzio A M, Dosen S, Lemling S, Markovic M, Schweisfurth M A, Ge N, Graumann B, Falla D
32
33 789 and Farina D 2017 Tactile feedback is an effective instrument for the training of grasping with a
34
35 790 prosthesis at low- and medium-force levels *Exp. Brain Res.* **235** 2547–59
36
37
38 791 [45] Farina D and Sartori M 2016 Surface Electromyography for Man-Machine Interfacing in
39
40 792 Rehabilitation Technologies *Surface Electromyography: Physiology, Engineering and Applications*
41
42 793 ed D Farina and R Merletti (IEEE/Wiley) pp 540–60
43
44 794 [46] Parker P, Englehart K and Hudgins B 2006 Myoelectric signal processing for control of powered
45
46 795 limb prostheses *J. Electromyogr. Kinesiol.* **16** 541–8
47
48 796 [47] Kuiken T, Turner K, Soltys N and Dumanian G 2015 First clinical fitting of an individual after
49
50 797 bilateral TMR with pattern recognition control *Prosthet. Orthot. Int.* **39** 133
51
52 798 [48] Hargrove L J, Miller L A, Turner K and Kuiken T A 2017 Myoelectric Pattern Recognition
53
54 799 Outperforms Direct Control for Transhumeral Amputees with Targeted Muscle Reinnervation: A
55
56 800 Randomized Clinical Trial *Sci. Rep.* **7**
57
58
59 801 [49] Hahne J M, Markovic M and Farina D 2017 User adaptation in Myoelectric Man-Machine Interfaces
60
61
802 *Sci. Rep.* **7**

- 1
2 803 [50] Eilenberg M F, Geyer H and Herr H 2010 Control of a powered ankle-foot prosthesis based on a
3 neuromuscular model. *IEEE Trans. Neural Syst. Rehabil. Eng.* **18** 164–73
4 804
5
6 805 [51] Fleischer C and Hommel G 2008 A Human – Exoskeleton Interface Utilizing Electromyography
7 *IEEE Trans. Robot.* **24** 872–82
8 806
9
10 807 [52] Cavallaro E E, Rosen J, Perry J C and Burns S 2006 Real-Time Myoprocessors for a Neural
11 Controlled Powered Exoskeleton Arm *IEEE Trans. Biomed. Eng.* **53** 2387–96
12 808
13
14 809 [53] Farina D, Vujaklija I, Sartori M, Kapelner T, Negro F, Jiang N, Bergmeister K, Andalib A, Principe
15
16 810 J and Aszmann O 2016 Man-Machine Interfacing With Discharge Timings of Spinal Motor Neurons
17
18 811 After Targeted Muscle Reinnervation *Nat. Biomed. Eng.*
19
20
21 812 [54] Formica D, Charles S K, Zollo L, Guglielmelli E, Hogan N and Krebs H I 2012 The passive stiffness
22 of the wrist and forearm *J. Neurophysiol.* **108** 1158–66
23
24
25 814 [55] Charles S K and Hogan N 2011 Dynamics of wrist rotations *J. Biomech.* **44** 614–21
26
27 815 [56] Rankin J W and Neptune R R 2012 Musculotendon lengths and moment arms for a three-
28 dimensional upper-extremity model. *J. Biomech.* **45** 1739–44
29 816
30
31 817 [57] Holzbaur K R S, Murray W M and Delp S L 2005 A Model of the Upper Extremity for Simulating
32
33 818 Musculoskeletal Surgery and Analyzing Neuromuscular Control *Ann. Biomed. Eng.* **33** 829–40
34
35
36 819 [58] Peaden A W and Charles S K 2014 Dynamics of wrist and forearm rotations *J Biomech* **47** 2779–85
37
38 820
39
40 821 **COMPETING INTERESTS**
41
42 822 The authors declare no financial competing interests.
43
44 823
45
46 824 **PARTICIPANT CONSENT**
47
48 825 The authors have confirmed that any identifiable participants in this study have given their consent for
49 publication.
50 826
51
52 827
53
54 828 **DATA AND MATERIALS AVAILABILITY**
55
56 829 Data and code are available upon request.
57
58
59 830
60
61 831 **MOVIES**

1
2 832 **Movie 1. Graphical user interface during wrist control tasks.** The proposed model-based framework
3
4 833 operated in real-time for the simultaneous control of the prosthesis wrist flexion-extension (WFE) and
5
6 834 pronation-supination (WPS) by IL1 (Table II). The movie displays the musculoskeletal model, recorded
7
8 835 EMGs and estimated joint moments (see laptop) and the concurrent control of the ball-shaped cursor for
9
10 836 reaching a variety of diagonal targets (see user interface on external screen). Note that the cursor diagonal
11
12 837 trajectories directly correspond to the prosthesis simultaneous actuation of WPS and WFE. After every target
13
14 838 is successfully reached, the prosthesis automatically resets to its neutral position.
15
16
17 839
18
19 840 **Movie 2. Non-sensorised clothespin test.** The transradial amputee subject picking and placing non-
20
21 841 sensorised pins arranged in four triplets of different stiffness as previously reported (22). The amputee
22
23 842 controls prosthesis wrist pronation-supination and hand opening-closing simultaneously while generating
24
25 843 natural motions.
26
27 844
28
29 845 **Movie 3. Sensorised clothespin test.** The transradial amputee subject picking and placing sensorised pins of
30
31 846 different stiffness. The target force windows to successfully relocate each pin are 7-15% (yellow pin), 13-
32
33 847 23% (red pin), 23-32% (green pin), and 35-43% (black pin) of the prosthesis maximum force. The movie
34
35 848 shows the amputee's ability of fine controlling the prosthesis grip force while simultaneously controlling
36
37 849 hand rotation, while not triggering the light sensor.
38
39
40 850
41
42 851 **Movie 4. Block turn test.** The transradial amputee executes a block-turn task involving fine control of
43
44 852 prosthesis wrist pronation-supination and hand opening-closing simultaneously in the precise positioning of
45
46 853 a narrow wooden block in equilibrium on a wooden shelf.
47
48 854
49
50 855 **Movie 5. Egg manipulation.** The transradial amputee precisely controls hand opening-closing grip force for
51
52 856 grasping an egg. The movie shows the amputee's ability of fine grasping force control while rotating the
53
54 857 prosthetic wrist without breaking the egg.
55
56
57 858
58
59 859 **Movie 6. Cable induced movement artefacts.** How our proposed system being transparent to mechanically
60
61 induced cable-related movement artifacts visibly present in the recorded electromyograms. Despite the

1
2 861 artificially induced noise condition the prosthesis does not inadvertently activate unwanted degrees of
3
4 862 freedom. The movie also shows amputee's voluntary prosthesis control under noise condition.
5
6 863
7
8 864

9 **Movie 7. Manipulation of heavy objects.** Our proposed system enabling grasping and manipulating heavy
10 865 objects including a 1.5L water bottle, a task that would be challenging for state of the art non-invasive
11
12 866 myoelectric systems.
13
14
15
16
17
18
19
20
21
22
23
24
25
26
27
28
29
30
31
32
33
34
35
36
37
38
39
40
41
42
43
44
45
46
47
48
49
50
51
52
53
54
55
56
57
58
59
60